Food Materials Research

ARTICLE

Open Access

https://doi.org/10.48130/FMR-2022-0014

Food Materials Research **2022**, 2:14

Optical and electrochemical dual detection of β-lactoglobulin based on the methylene blue@copper-based metal-organic framework

Yuwei Wang[1#], Jingyi Hong[1#], Xinlong Wang[1], Liying Zhu[2*], and Ling Jiang[1,3*]

[1] *College of Food Science and Light Industry, State Key Laboratory of Materials-Oriented Chemical Engineering, Nanjing Tech University, Nanjing 211816, China*
[2] *School of Chemistry and Molecular Engineering, Nanjing Tech University, Nanjing 211816, China*
[3] *State Key Laboratory of Materials-Oriented Chemical Engineering, Nanjing Tech University, Nanjing 211816, China*
[#] These authors contributed equally: Yuwei Wang, Jingyi Hong
[*] Corresponding author, E-mail: zlyhappy@njtech.edu.cn; jiangling@njtech.edu.cn

Abstract

β-lactoglobulin is an effective indicator of allergic protein detection. Herein, we produced a copper-based metal-organic framework coated with methylene blue, to realize the optical and electrochemical dual detection of β-lactoglobulin. Methylene blue was successfully encapsulated inside the copper-based metal-organic framework and released after addition of β-lactoglobulin. As the concentration of β-lactoglobulin increased, the intensity of the ultraviolet absorption band and the response current increased with the increasing concentration of methylene blue released from the copper-based metal-organic framework. The optical detection range is from 0.10 mg/mL to 10 mg/mL, and the detection limit is 0.10 mg/mL. The electrochemical detection range is from 1.0×10^{-7} mg/mL to 8.0×10^{-7} mg/mL, the detection limit is 2.0×10^{-8} mg/mL. The dual detection strategy, with no interfere with each other, played a synergetic role in the quick qualitative and precise quantitative analyses of β-lactoglobulin in a wide range of applications.

Citation: Wang Y, Hong J, Wang X, Zhu L, Jiang L. 2022. Optical and electrochemical dual detection of **β**-lactoglobulin based on the methylene blue@copper-based metal-organic framework. *Food Materials Research* 2:14 https://doi.org/10.48130/FMR-2022-0014

INTRODUCTION

Food allergies have attracted increasing public attention recently for their influence on food safety and public health. At present, avoiding the intake of allergens is still the only effective way to prevent food allergies[1]. Among infants and young children, cow's milk protein allergy (CMPA) is defined as the most common food allergy, affecting around 2.5% of young children in the first 2 years of life[2]. β-lactoglobulin (β-Lg) is one of the most important allergic proteins in cow's milk[3]. It is reported that about 82% of CMPA is triggered by β-Lg in milk proteins[4]. Dairy products nowadays have become common dietary ingredients, and the prevalence of related chronic conditions is still on the rise. Therefore, the detection of β-Lg in food has become an important part of the prevention and control of the allergy.

To date, many methods have been developed for detection of β-Lg, including 1) immunological detection technologies, for instance, enzyme linked immuno sorbent assay (ELISA)[5,6], immunochromtogaphic assa (ICA)[7], immunoblotting technique (IBT)[8,9], and immune biosensor technique[10], 2) chromatographic detection technologies, such as ultra performance liquid chromatography (UPLC)[11], high performance liquid chromatography (HPLC)[12], and 3) molecular biological detection methods, including polymerase chain reaction (PCR) and loop-mediated isothermal amplification (LAMP)[13]. However, these conventional detection methods still have several disadvantages, such as expensive equipment, tedious operation and high personnel requirements. Recently, electrochemical sensors have become one of the preferred technologies, due to its easy modification, simple operation, fast response, high sensitivity, and low cost[14,15]. Surucu et al.[16] determined the redox behavior of β-LG over H_2O_2 by using a graphene oxide modifing the disposable pencil graphite electrode. Xu et al.[17] produced flower-like bismuth vanadate microspheres applied in the construction of electrochemical biosensors with highly selective aptamers to detect β-Lg.

In a previous study, we prepared multi-modified screen-printed electrodes (SPEs) using polyethyleneimine (PEI)-reduced graphene oxide (rGO)-gold nanoclusters (AuNCs) which performed well in the detection of β-Lg[18] with excellent electrical conductivity. Nevertheless, the morphology of AuNCs is hard to control, which would affect the performance of the electrodes. Finding an alternative material is therefore important. Coincidentally, in recent research, metal-organic frameworks (MOFs) have attracted much attention, formed by metal ions or metal clusters and organic ligands with clear pore structure, large surface area and flexible structure. The pore space of MOFs can be modified to combine with different substances to afford special restrictions, such as carbon nanostructures, metal complexes, polymers, organic dyes, biomolecules, porphyrins and so on[19]. By encapsulating these materials in a cavity, MOFs provides new functional materials for applications such as sensing[20], heterogeneous catalysis[21], loading and controlled release of drug molecules[22,23]. Qin et al.[20] constructed a self-

assembled zinc zeolite imidazole framework (ZIF-8) of zinc ion and 2-methylimidazole coated with ferrocene with optical and electrochemical activity, which can be used for the dual detection of amyloid β-oligomers, the main neuropathological marker of Alzheimer's4 disease. In the case of MOFs in drug loading and sustained release, Taylor-Pashow et al.[24] introduced the Fe(III)-carboxylate nanoscale metal-organic frameworks (NMOFs) with ethoxysuccinato-cisplatin anticancer prodrug and optical contrast agent (a BODIPY dye) inside via the postsynthetic modifications of the as-synthesized particles, which were released upon the degradation of NMOFs, and made further efforts to control the release rate of these cargo by coating the NMOF particles with a silica shell.

Inspired by the sustained drug release with MOF, we designed a signal probe with copper-based metal-organic framework (Cu-MOF) as the carrier, and the structure can be decomposed by β-Lg and release the signal probe. Methylene blue (MB) was then encapsulated and coated with MOF to form MB@Cu-MOF for the finally quantitative determination of β-Lg. The concentration of the released MB was linearly proportional to the β-Lg content, as determined by UV/vis spectrophotometry, differential pulse voltammetry (DPV) and cyclic voltammetry (CV). This is a new and robust way for the dual detection of β-Lg, combining both the optical and electrochemical sensing strategy to play a synergetic role in the quick qualitative analysis and precise quantitative detection of β-Lg. Furthermore, the dual detection of β-Lg shows a high flexibility in the face of different detection needs in a practical approach.

RESULTS AND DISCUSSION

Strategy of optical and electrochemical dual detection

An optical and electrochemical dual measurement method was developed with MB@Cu-MOF. The functional mechanism of this sensor is shown in Fig. 1. Cu^{2+} with electrical activity in Cu-MOF would produce high electrochemical signals in signal transduction for its good redox activity. What's more, MB has both optical and electrochemical activities[25–27]. MB@Cu-MOF was obtained by encapsulating MB inside the Cu-MOF as an indicator before the self-installation of Cu-MOF[28]. However, when β-Lg is added into this system, the structure of the original MOF would be destroyed. This is due to the fact that the binding ability of β-Lg to imidazole is greater than that of copper ion to imidazole. As a result, the internally encapsulated MB could be released, and optical and electrochemical dual detection of β-Lg can be achieved.

Coordination of MB with copper chloride

We used ultraviolet-visible (UV-vis) spectrum to monitor the gradual encapsulation of MB. In Fig. 2, the characteristic peak of MB is at 663 nm[29]. After the addition of copper chloride ($CuCl_2{\cdot}2H_2O$), the characteristic peak has a slight blue shift, which can be attributed to the weak coordination between MB and the copper ion.

Characterization of Cu-MOF and MB@Cu-MOF

MOFs are often used in the fields of adsorption separation[30], gas storage[31] and drug delivery[32]. Owing to

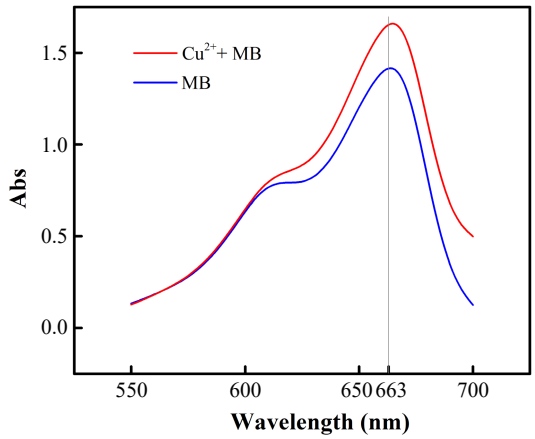

Fig. 2 The UV-vis spectra of MB solution and mixed solution of MB and copper chloride.

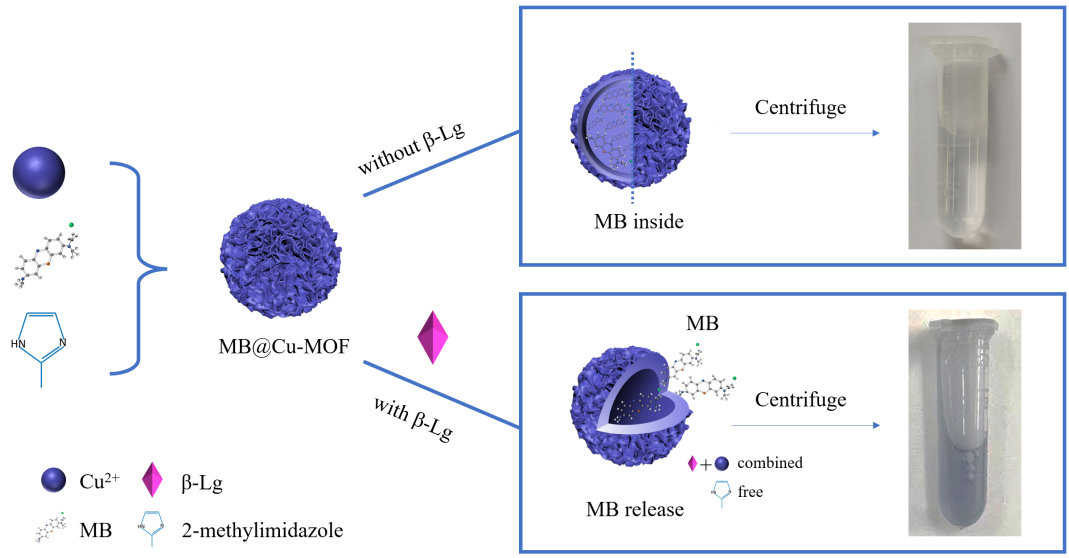

Fig. 1 Schematic diagram of measuring β-Lg by MB@Cu-MOF electrochemistry.

the high adsorption capability, MOFs could adsorb structures on its surface. However, in our study, MB need to be encapsulated in the interior of MOFs instead of their surface. To achieve this, we added MB before the combination of copper ion and methylene imidazole to make MB encapsulated in the process of the MOF formation. In order to confirm the production of the above materials, the following methods were used to characterize the Cu-MOF and the MB@Cu-MOF.

The functional groups in Cu-MOF, MB@Cu-MOF were analyzed by fourier transform infrared (FTIR). In Fig. 3a, the absorption peaks at 1,420 cm^{-1}, 1,150 cm^{-1} can be assigned to the C-H stretching vibration in 2-methylimidazole, and several major bands between bands at 2,990 cm^{-1} and 2,950 cm^{-1} are ascribed to the characteristic stretching vibration modes of C-H in methyl and methylene. In addition, the peak at 3,470 cm^{-1} of the sample may be caused by water absorption. Notably, the characteristic peaks in the infrared spectra of Cu-MOF and MB@Cu-MOF are basically the same, which can preliminarily prove that MB has been encapsulated in the interior of Cu-MOF.

The crystal structures of Cu-MOF and MB@Cu-MOF were observed by X-Ray Diffractometer (XRD). As shown in Fig. 3b, the diffraction peaks of Cu-MOF and MB@Cu-MOF are mainly distributed at 15.92°, 31.32° and 34.86°. The diffraction intensity of the diffraction peaks at 31.32° and 34.86° are weak and the crystal size is small. We speculate that trace amounts of copper oxide (CuO) were the consequence of water absorption. The peaks of Cu-MOF and MB@Cu-MOF are similar, indicating that the encapsulation of MB does not affect the crystal form of Cu-MOF, which further verified that MB is located in the pores of Cu-MOF rather than physically adsorbed on the surface.

MB@Cu-MOF was presented in the form of blue-black solid powder, and Cu-MOF in the form of khaki solid powder as shown in Fig. 3c and d. In order to characterize the morphology of the Cu-MOF and MB@Cu-MOF, we analyzed these two materials by SEM. It can be seen from Fig. 3c that the structure of Cu-MOF is spherical, formed by the accumulation of nano-sheets, which is also similar to that of MB@Cu-MOF. The average particle size both Cu-MOF and MB@Cu-MOF of 400–500 nm was calculated based on SEM images.

As we can see by the above experimental results, the encapsulation of MB does not affect the basic structure and morphology of Cu-MOF, and this can also confirm that MB does exist in the interior of MOF materials instead of being adsorbed on the surface.

Performance characterization of the sensor

The performance of β-Lg detection with our sensor can be evaluated from the UV-vis spectrum, CV and SEM. As shown in Fig. 4a, the peak patterns of Cu-MOF and MB@Cu-MOF are similar, but they have no characteristic absorption peak at 663 nm as seen in MB, indicating that there is no free MB in MB@Cu-MOF solution. However, by incubating MB@Cu-MOF with β-Lg to destroy the Cu-MOF structure, a peak at 663 nm

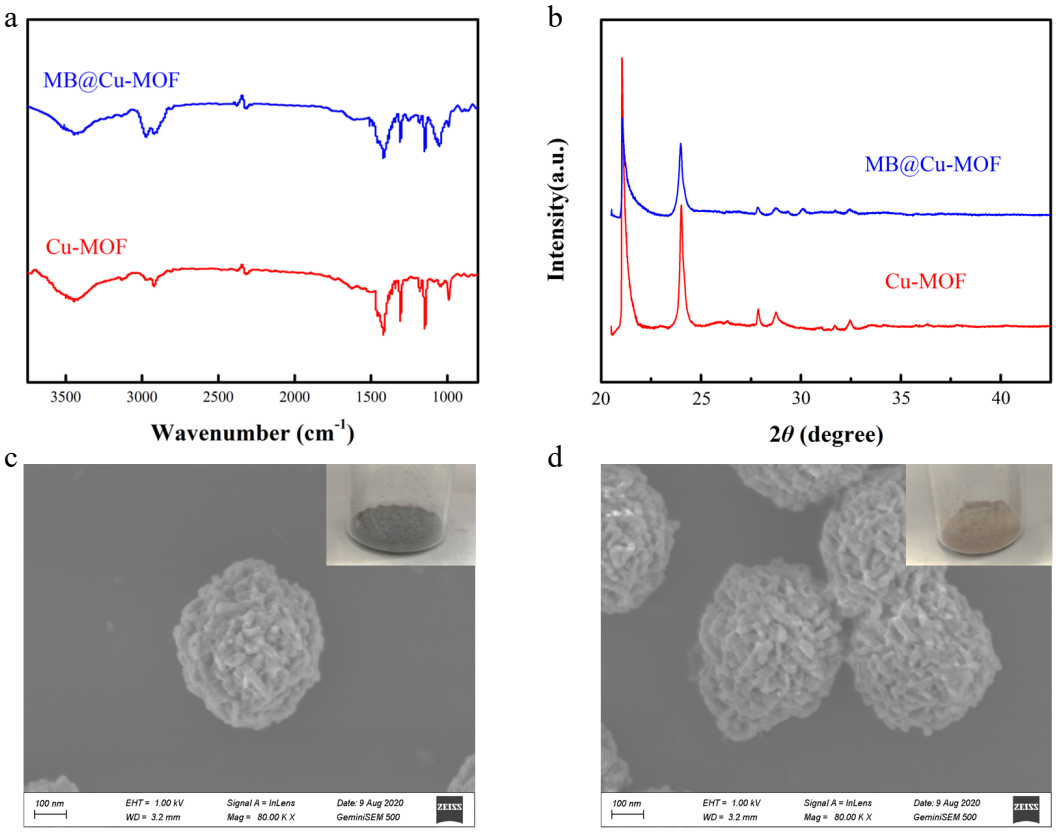

Fig. 3 (a) FTIR spectrum and (b) X-ray diffraction of the Cu-MOF and the MB@Cu-MOF. SEM images of (c) the Cu-MOF and (d) the MB@Cu-MOF.

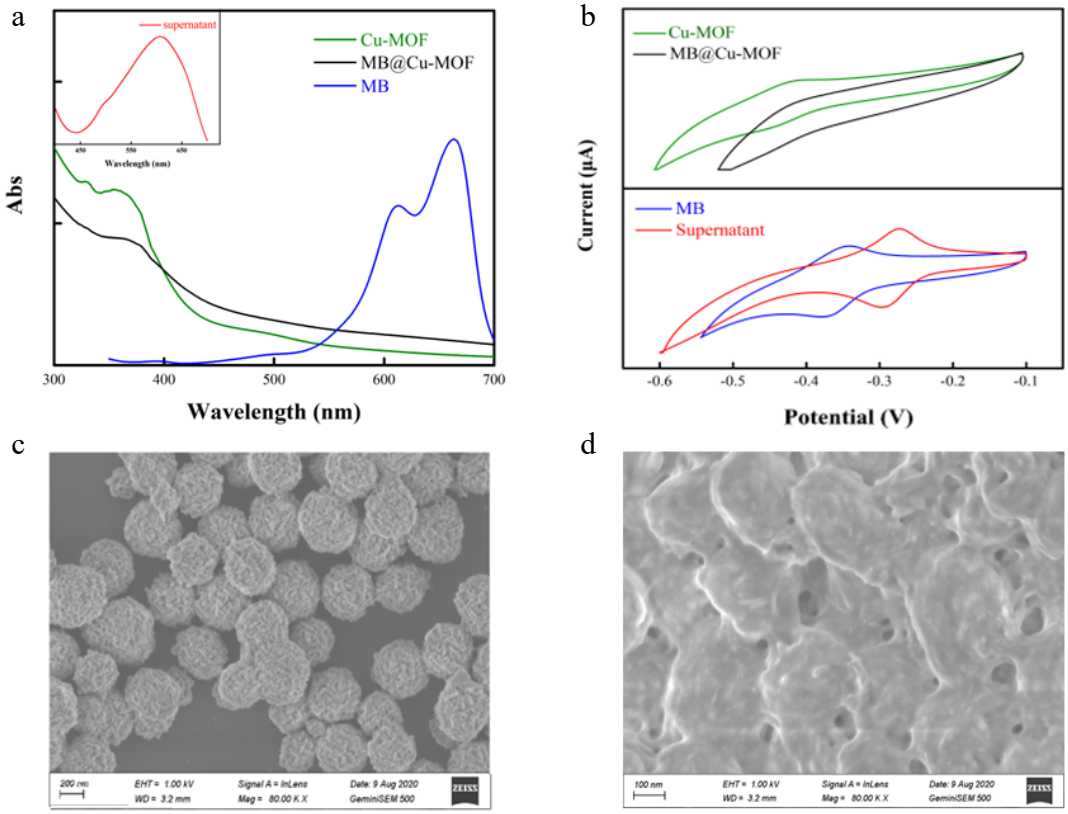

Fig. 4 (a) UV-Vis and (b) cyclic voltammogram of the MB, the Cu-MOF, the MB@Cu-MOF and the supernatant. SEM images of (c) the MB @ Cu-MOF and (d) the MB@Cu-MOF incubation with β-Lg.

can be obtained (Fig. 4a). Besides, Cu-MOF and MB@Cu-MOF have no redox activity, so they do not have a redox peak in the range of −0.6 V ~ −0.1 V (Fig. 4b), but the samples with β-Lg have a redox peak similar to MB. Figure 4c shows the SEM picture of MB@Cu-MOF, and Fig. 4d shows the SEM picture of MB@Cu-MOF incubated with β-Lg. After β-Lg was incubated with MB@Cu-MOF, MB@Cu-MOF no longer had a regular structure. Because the binding force of Cu^{2+} to β-Lg is greater than that of Cu^{2+} to imidazole, the original Cu-MOF structure was destroyed, and the surface became rough and the outline was also blurred. It can be deduced that β-Lg destroyed the structure of MB@Cu-MOF. After incubating MB@Cu-MOF with β-Lg, MB encapsulated in MB@Cu-MOF was released, and the supernatant obtained by centrifugation was blue, which also proved that MB was contained in the supernatant. The samples can be indirectly detected and analyzed by electrochemical analysis instruments and UV-vis spectrometer at the same time, which proves the feasibility of the sensor detection.

Detection of β-Lg by sensors

Figure 5 shows the standard curve of MB aqueous solution on UV-vis spectra and DPV, respectively, to facilitate the subsequent indirect detection of β-Lg using optical electrochemistry. Fluorescent techniques were conducted for MB, Cu-MOF, and MB@ Cu-MOF, individually (Supplemental Fig. S1), to gain more information about the preparation of MB@Cu-MOF and to disclose MB's dual-signal property[33]. The supernatant obtained after the incubation of MB@Cu-MOF with β-Lg and the centrifugation was analyzed by UV-vis absorption spectrum, in the wavelength range of 400–700 nm (Fig. 6a). Obviously, the absorption band intensity of the characteristic peak of the supernatant increased with the increase of β-Lg concentration, showing a linear relationship in the range of 0.1–10 mg/mL. The linear regression equation was Y = 0.0517 + 0.02166 X, the correlation coefficient (R^2) was 0.9878 and the LOD was 0.1 mg/mL (S/N = 3).

MB not only has optical activity, but also has electrochemical activity. We made use of the electrochemical activity of MB to further narrow the detection range of β-Lg. As shown in Fig. 6b, with the increase of β-Lg concentration, the DPV response current of the supernatant increased in the range of 1×10^{-7} mg/mL to 8×10^{-7} mg/mL. The linear regression equation was Y = 5.628 + 0.2057 X, the correlation coefficient (R^2) was 0.9903 and the LOD was 2×10^{-8} mg/mL (S/N = 3). The detection by electrochemical analysis shows higher sensitivity in a wider detection range.

The specificity of MB@Cu-MOF to β-Lg

β-Lg is the main indicator in the detection of milk allergens, however, considering the complex composition of cow's milk, α-lactalbumin (α-La), lysozyme, bovine serum albumin (BSA) and casein are often regarded as interfering substances in the process of specific detection. The amino acid composition of β-Lg in the literature shows the presence of two acidic amino acids carrying a negative charge[34]. It has been shown that several positive metal ions, including Cu^{2+}, have an affinity for certain proteins[35–37]. What's more, in the interactions between β-Lg with these divalent metal ions, the effect of copper ion-induced aggregation of β-Lg is much stronger

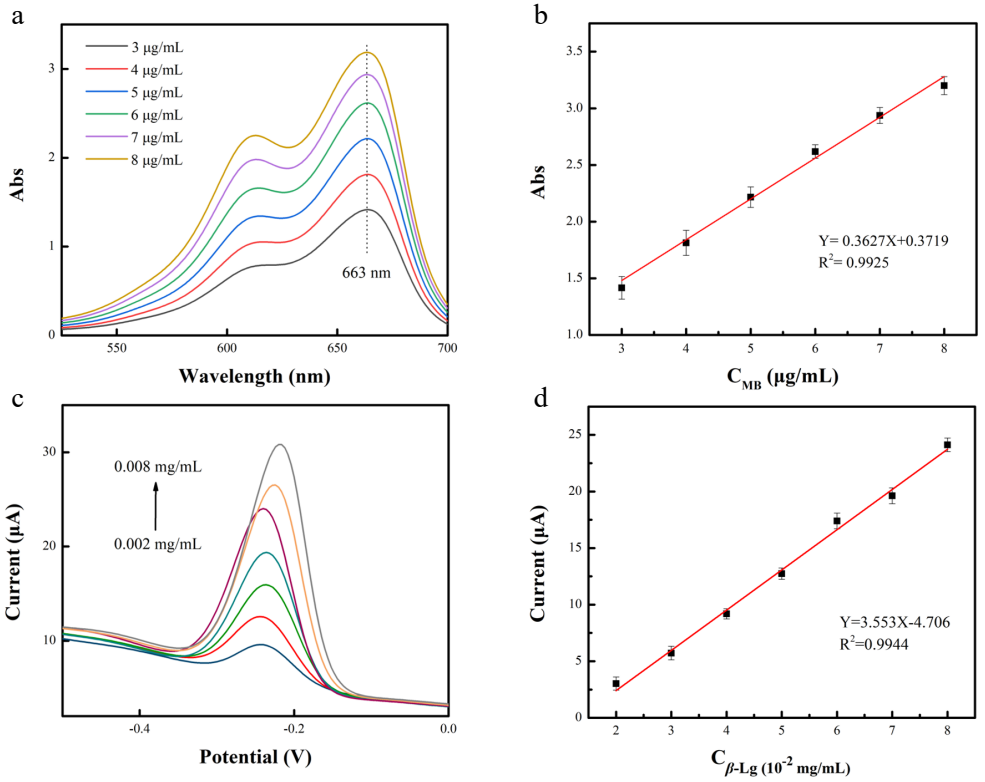

Fig. 5 (a) UV-vis absorption spectra and differential pulse voltammograms of different concentrations of MB. (b) Standard curves of MB on UV-vis spectra and differential pulse voltammetry curves.

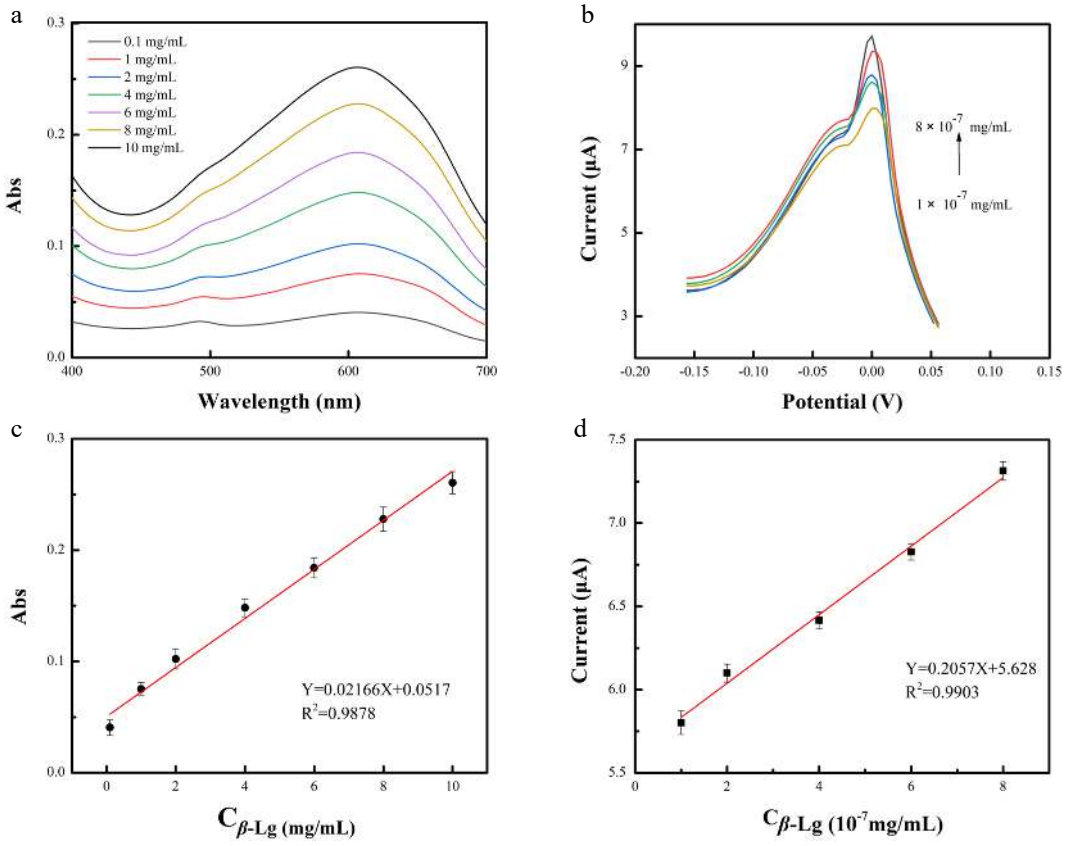

Fig. 6 (a) UV-vis and (b) differential pulse voltammetry (DPV) of the supernatant after incubation with different concentrations of β-Lg and MB@Cu-MOF. Standard curve of logarithm of β-Lg concentration on (c) UV-vis spectrum and (d) DPV curve.

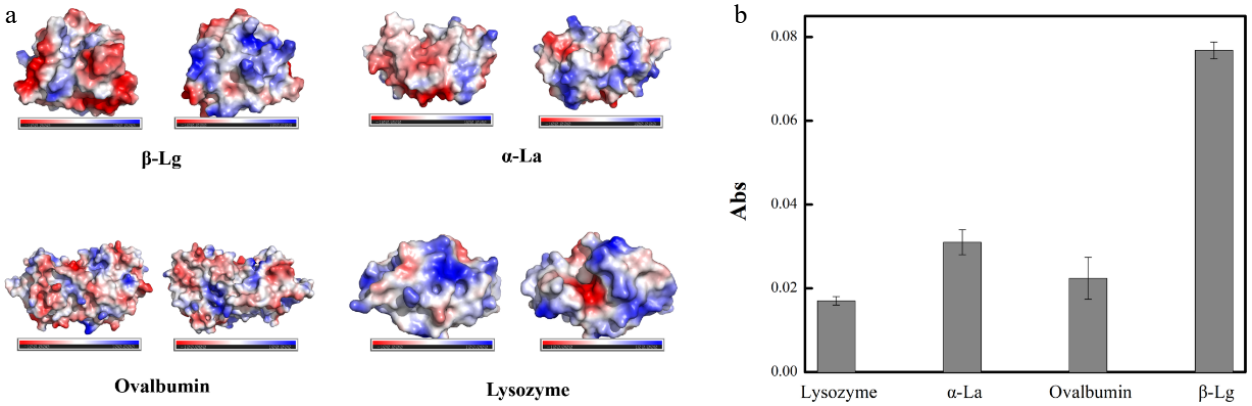

Fig. 7 (a) The nature and distribution of surface charge of β-Lg, lysozyme, α-La and ovalbumin. (b) The absorbance of the MB@Cu-MOF incubation with β-Lg (1 mg/mL), lysozyme (1 mg/mL), α-La (1 mg/mL) and Ovalbumin (1 mg/mL).

than that of the other metal ions, which is the reason for our choice of copper ion[38].

Combined with the structure diagram of the proteins given in Fig. 7a, the type and shade of the colour show the nature and distribution of surface charge. UV-vis spectrum was used to compare the supernatant of MB@Cu-MOF incubated with these proteins. One mg/mL of β-lg, lysozyme, α-La, and ovalbumin were prepared with 3 mg/mL MB@Cu-MOF in a 1:1 volume ratio, respectively, after which they were incubated at 25 °C for 60 min, and the supernatant obtained after centrifugation was measured under UV-vis spectrum. As illustrated in Fig. 7b, interfering substances (1 mg/mL) did not exhibit significant absorbance, and relevant variation were less than 0.04. However, the absorbance (0.0768) was observed in the presence of β-Lg. The results indicated that the absorbance of interfering substances was lower than that of β-Lg, which further confirmed the specificity of MB@Cu-MOF to the target.

Milk sample analysis

In order to test the ability of the modified electrode to detect β-Lg in real samples, the developed electrochemical sensors were used in pure milk samples to detect β-Lg of four brands common available on the market. As shown in Table 1, electrochemical sensors and ELISA showed relatively similar results, indicating that the sensors can be routinely used for the measurement of β-Lg. Furthermore, the detection limit of the ELISA is at least 2×10^{-2} mg/mL, whereas the detection limit of the modified sensor is 2×10^{-8} mg/mL.

CONCLUSIONS

We fabricated a sensor material MB@Cu-MOF, and successfully realized the optical and electrochemical double detection of β-Lg, with a wide detection range, simple synthetic method for modified electrode and low cost. In addition, the sensor prepared in this paper is small enough to carry easily, which is expected to be used in the manufacture of portable detection equipment. Moreover, the prepared sensors had good performance in detection of β-Lg in real samples, and showed great potential in practical application. This material is also expected to be used for the detection of other biomolecules, providing a new idea for electrochemical sensing detection.

Table 1. Comparison of β-Lg detection in real samples using the ELISA and modified sensors.

Sample	ELISA (μg/mL)	Modified sensor (μg/mL)
Telunsu	17.09 ± 0.56	17.05 ± 0.55
Yili	15.54 ± 0.47	16.10 ± 0.10
Mengniu	15.47 ± 0.40	14.60 ± 0.60
Jindian	10.38 ± 0.02	10.85 ± 0.25

EXPERIMENTAL

Reagents and materials

Copric chloride dihydrate ($CuCl_2 \cdot 2H_2O$, AR) was purchased from Meryer Chemical Technology Co., Ltd (Shanghai, China). Methylene blue (MB, AR) was obtained from Alfa Aesar (Shanghai, China). 2-methylimidazole ($C_4H_6N_2$, AR), β-Lg (99%) and methanol (CH_3OH) were all obtained from Aladdin Reagent Co., Ltd (Shanghai, China). Hexadecyl trimethyl ammonium bromide (CTAB, AR) was purchased from Jiangsu Yonghua Fine Chemical Co., Ltd (Shanghai, China). Potassium dihydrogen phosphate (KH_2PO_4, AR) and Dipotassium hydrogenphosphate (K_2HPO_4, AR) were purchased from Xilong Scientific Co. Ltd (Guangzhou, China). Potassium chloride (KCl, AR), potassium ferricyanide ($K_3[Fe(CN)_6]_3$, AR) and Potassium hexacyanoferrate(II) ($K_4[Fe(CN)_6]$, AR) were obtained from Sangon Biotech Co., Ltd. (Shanghai, China). Potassium bromide (KBr, AR) was obtained from Sinopharm Chemical Reagent Co., Ltd. (Shanghai, China).

Apparatus

Lambda 25 ultraviolet-visible (UV-vis) spectrometer (PerkinElmer lambda, USA) were used to record the UV-vis absorption spectra. The CHI 660E electrochemical workstation (Shanghai Chenhua Instrument Co., Ltd., Shanghai, China) was used to carry out all the electrochemical measurements. NPTY0569 disposable screen printing electrode were purchased from NEOPRO Biotechnologies Co., Ltd. (Shandong, China), and the sensor connector (NEOPRO Biotechnologies Co., Ltd.) allows the screen printing electrode to be connected to the electrochemical workstation. The SU8010 scanning electron microscope (HITACHI, Japan) was used to determine the morphology of the synthetized material. The

Bruker EDS QUANTAX energy dispersive spectrometer (Bruker Daltonics, Germany) cooperated with the SU8010 scanning electron microscope area was used to analyze the type and content of elements in the material micro area. Infrared spectrum were recorded using a VERTEX 33 fourier transform infrared (FTIR) spectrometer (Bruker Daltonics Inc, Germany). The D8advannce X-Ray Diffractometer (XRD) was purchased from Bruker Daltonics Inc, Switzerland.

Synthesis of MB@Cu-MOF

MB@Cu-MOF was synthesized by one-pot reaction. Copper chloride was dispersed in ultrapure water (50 mM, 20 mL), and MB (56 mL) was added under intense stirring. After 10 min, 2-methylimidazole (0.97 M, 20 mL) and hexadecyl trimethyl ammonium bromide (0.96 mM, 20 mL) were added successively. The mixture was stirred for 60 min to form blue-black precipitation, washed with methanol several times until the supernatant was colorless and transparent. And then the precipitation was freeze-dried for 36 h to obtain blue-black powder. The amount of MB coated by Cu-MOF was adjusted by changing the concentration of MB solution. According to the above method, Cu-MOF, without MB was synthesized by a similar method for comparison.

Characterization

Material

The synthesized materials were analyzed by XRD, FTIR absorption spectroscopy. The scanning electron microscope (SEM) was used to characterize the surface morphology of Cu-MOF and MB@Cu-MOF.

Performance of sensor connector

The optical detection was carried out by UV-vis spectrometer and the electrochemical experiment was carried out using an electrochemical workstation. The electrochemical experimental phenomena were observed by cyclic voltammetry (CV)[39] and differential pulse voltammetry (DPV)[40].

Electrochemical assay method of β-Lg

For the detection of β-Lg, potassium ferricyanide solution dissolved in phosphate buffer solution (PBS, 0.10 M) was selected as the supporting electrolyte, and the CV curve and DPV curve between −0.60 V and −0 V were recorded by DPV. All electrochemical measurements were carried out at room temperature using CV, DPV, and all were performed in PBS, containing 1.0 mM $K_4Fe(CN)_6$, 5.0 mM $K_3[Fe(CN)_6]$ and 0.1 mmol/L KCl, according to the reported literature[18]. The parameters used for the DPV measurements: Inter Electromotive force: −0.60 V; Final Electromotive force: 0.10 V; Amplitude: 0.050 V; Pulse width: 0.050 s; Pulse period: 0.20 s.

ACKNOWLEDGMENTS

This work was supported by the National Key R&D Program of China (2017YFC1600404), the National Natural Science Foundation of China (31922070, U2106228), and the Jiangsu Synergetic Innovation Center for Advanced Bio-Manufacture (XTC2205).

Conflict of interest

The authors declare that they have no conflict of interest.

Supplementary Information accompanies this paper at (http://www.maxapress.com/article/doi/10.48130/FMR-2022-0014)

Dates

Received 31 May 2022; Accepted 23 August 2022; Published online 9 September 2022

REFERENCES

1. Sena-Torralba A, Pallás-Tamarit Y, Morais S, Maquieira Á. 2020. Recent advances and challenges in food-borne allergen detection. *Trends in Analytical Chemistry* 132:116050
2. Sicherer SH, Sampson HA. 2014. Food allergy: Epidemiology, pathogenesis, diagnosis, and treatment. *The Journal of Allergy and Clinical Immunology* 133:291–307. E5
3. Blanc F, Bernard H, Alessandri S, Bublin M, Paty E, et al. 2008. Update on optimized purification and characterization of natural milk allergens. *Molecular Nutrition & Food Research* 52:S166–S175
4. Villa C, Costa J, Oliveira MBPP, Mafra I. 2018. Bovine milk allergens: A comprehensive review. *Comprehensive Reviews in Food Science and Food Safety* 17:137–64
5. He S, Li X, Gao J, Tong P, Chen H. 2017. Development of sandwich ELISA for testing bovine β-lactoglobulin allergenic residues by specific polyclonal antibody against human IgE binding epitopes. *Food Chemistry* 227:33–40
6. He S, Li X, Wu Y, Wu S, Wu Z, et al. 2018. A novel sandwich enzyme-linked immunosorbent assay with covalently bound monoclonal antibody and gold probe for sensitive and rapid detection of bovine β-lactoglobulin. *Analytical and Bioanalytical Chemistry* 410:3693–703
7. Wu X, He W, Ji K, Wan W, Hu D, et al. 2013. A simple and fast detection method for bovine milk residues in foods: A 2-site monoclonal antibody immunochromatography assay. *Journal of Food Science* 78:M452–M457
8. Haneda Y, Kadowaki S, Furui M, Taketani T. 2021. A pediatric case of food-dependent exercise-induced anaphylaxis due to rice bran. *Asia Pacific Allergy* 11:e4
9. Fiocchi A, Restani P, Bernardini R, Lucarelli S, Lombardi G, et al. 2006. A hydrolysed rice-based formula is tolerated by children with cow's milk allergy: A multi-centre study. *Clinical & Experimental Allergy* 36:311–16
10. Wang W, Zhu X, Teng S, Xu X, Zhou G. 2018. Development and validation of a surface plasmon resonance biosensor for specific detection of porcine serum albumin in Food. *Journal of AOAC International* 101:1868–72
11. Qi K, Liu T, Yang Y, Zhang J, Yin J, et al. 2019. A rapid immobilized trypsin digestion combined with liquid chromatography – Tandem mass spectrometry for the detection of milk allergens in baked food. *Food Control* 102:179–87
12. Terheggen-Lagro SWJ, Khouw IMSL, Schaafsma A, Wauters EAK. 2002. Safety of a new extensively hydrolysed formula in children with cow's milk protein allergy: A double blind crossover study. *BMC Pediatrics* 2:10
13. Allgöwer S, Hartmann CA, Lipinski C, Mahler V, Randow S, et al. 2020. LAMP-LFD based on isothermal amplification of multicopy gene *ORF160b*: Applicability for highly sensitive low-tech screening of allergenic soybean (*Glycine max*) in food. *Foods* 9:1741
14. Ronkainen NJ, Halsall HB, Heineman WR. 2010. Electrochemical biosensors. *Chemical Society Reviews* 39:1747–63
15. Ruiz-Valdepenas Montiel V, Campuzano S, Conzuelo F, Torrente-Rodríguez RM, Gamella M, et al. 2015. Electrochemical magnetoimmunosensing platform for determination of the milk allergen beta-lactoglobulin. *Talanta* 131:156–62

16. Surucu O, Abaci S. 2019. Electrochemical determination of β-lactoglobulin in whey proteins. *Journal of Food Measurement and Characterization* 14:11–19
17. Xu S, Dai B, Zhao W, Jiang L, Huang H. 2020. Electrochemical detection of beta-lactoglobulin based on a highly selective DNA aptamer and flower-like Au@$BiVO_4$ microspheres. *Analytica Chimica Acta* 1120:1–10
18. Hong J, Wang Y, Zhu L, Jiang L. 2020. An electrochemical sensor based on gold-nanocluster-modified graphene screen-printed electrodes for the detection of β-lactoglobulin in Milk. *Sensors* 20:3956
19. Liu L, Zhou Y, Liu S, Xu M. 2018. The applications of metal-organic frameworks in electrochemical sensors. *ChemElectroChem* 5:6–19
20. Qin J, Cho M, Lee Y. 2019. Ferrocene-encapsulated Zn zeolitic imidazole framework (ZIF-8) for optical and electrochemical sensing of amyloid-beta oligomers and for the early diagnosis of alzheimer's disease. *ACS Applied Materials & Interfaces* 11:11743–48
21. Lee J, Farha OK, Roberts J, Scheidt KA, Nguyen ST, et al. 2009. Metal-organic framework materials as catalysts. *Chemical Society Reviews* 38:1450–59
22. Horcajada P, Serre C, Vallet-Regí M, Sebban M, Taulelle F, et al. 2006. Metal-organic frameworks as efficient materials for drug delivery. *Angewandte Chemie International Edition* 45:5974–78
23. An J, Geib SJ, Rosi NL. 2009. Cation-triggered drug release from a porous zinc-adeninate metal-organic framework. *Journal of the American Chemical Society* 131:8376–77
24. Taylor-Pashow KML, Della Rocca J, Xie Z, Tran S, Lin W. 2009. Postsynthetic modifications of iron-carboxylate nanoscale metal-organic frameworks for imaging and drug delivery. *Journal of the American Chemical Society* 131:14261–63
25. Guo J, Yuan C, Yan Q, Duan Q, Li X, et al. 2018. An electrochemical biosensor for microRNA-196a detection based on cyclic enzymatic signal amplification and template-free DNA extension reaction with the adsorption of methylene blue. *Biosensors and Bioelectronics* 105:103–8
26. Ma X, Qian K, Ejeromedoghene O, Kandawa-Schulz M, Song W, et al. 2021. p-Co-BDC/AuNPs-based multiple signal amplification for ultra-sensitive electrochemical determination of miRNAs. *Analytica chimica acta* 1183:338979
27. Patir A, Hwang GB, Nair SP, Allan E, Parkin IP. 2018. Photobactericidal activity of dual dyes encapsulated in silicone enhanced by silver nanoparticles. *ACS Omega* 3:6779–86
28. Chen C, Li N, Wang B, Yuan S, Yu L. 2020. Advanced pillared designs for two-dimensional materials in electrochemical energy storage. *Nanoscale Advances* 2:5496–503
29. Alshehri AA, Malik MA. 2020. Facile one-pot biogenic synthesis of Cu-Co-Ni trimetallic nanoparticles for enhanced photocatalytic dye degradation. *Catalysts* 10:1138
30. Singh S, Kaushal S, Kaur J, Kaur G, Mittal S, et al. 2021. CaFu MOF as an efficient adsorbent for simultaneous removal of imidacloprid pesticide and cadmium ions from wastewater. *Chemosphere* 272:129648
31. Dincă M, Long JR. 2008. Hydrogen storage in microporous metal-organic frameworks with exposed metal sites. *Angewandte Chemie (International ed. in English)* 47:6766–79
32. Xue S, Zhou X, Sang W, Wang C, Lu H, et al. 2021. Cartilage-targeting peptide-modified dual-drug delivery nanoplatform with NIR laser response for osteoarthritis therapy. *Bioactive Materials* 6:2372–89
33. Chang J, Lv W, Li Q, Li H, Li F. 2020. One-step synthesis of methylene blue-encapsulated zeolitic imidazolate framework for dual-signal fluorescent and homogeneous electrochemical biosensing. *Analytical Chemistry* 92:8959–64
34. Farrell HM Jr, Jimenez-Flores R, Bleck GT, Brown EM, Butler JE, et al. 2004. Nomenclature of the proteins of cows' milk - sixth revision. *Journal of Dairy Science* 87:1641–74
35. Yamanaka Y, Matsugano S, Yoshikawa Y, Orino K. 2016. Binding analysis of human immunoglobulin G as a zinc-binding protein. *Antibodies* 5:13
36. Marx PF, Bouma BN, Meijers JCM. 2002. Role of zinc ions in activation and inactivation of thrombin-activatable fibrinolysis inhibitor. *Biochemistry* 41:1211–16
37. Datta S, Leberman R, Rabin B. 1959. Relationship between proton and metal binding by some peptides, amino-acid amides and amino-acids. *Nature* 183:745–46
38. Arancibia V, Peña C, Segura R. 2006. Evaluation of powdered infant formula milk as chelating agent for copper under simulated gastric conditions of a baby's stomach. *Analytical Sciences* 22:1197–200
39. Eccles GN. 1991. Recent advances in pulse cyclic and square-wave cyclic voltammetric analysis. *Critical Reviews in Analytical Chemistry* 22:345–80
40. Lovrić M, Osteryoung J. 1982. Theory of differential normal pulse voltammetry. *Electrochimica Acta* 27:963–68